PHYSICAL REVIEW B VOLUME 58, NUMBER 11 15 SEPTEMBER 1998-I

# Sulfur-related metastable luminescence center in silicon

P. W. Mason,* H. J. Sun,† B. Ittermann,‡ S.S. Ostapenko,§ and G. D. Watkins
*Department of Physics, Lehigh University, Bethlehem, Pennsylvania 18015*

L. Jeyanathan,‖ M. Singh,¶ G. Davies, and E.C. Lightowlers
*Physics Department, King's College London, Strand, London WCR 2LS, United Kingdom*

(Received 1 April 1998)

Optical detection of magnetic resonance (ODMR) and photoluminescence (PL) studies are described for the sulfur-related metastable defect in silicon first reported by Brown and Hall. It is established that its two configurations, $A$ and $B$, are of triclinic ($C_1$) symmetry, and the incorporation of a single impurity atom with nuclear spin $I=3/2$ is confirmed directly by resolving its hyperfine structure in each ODMR spectrum. Detailed study of the conversion kinetics indicates the dominant $A\rightarrow B$ mechanism under below band-gap excitation to be the result of direct optical excitation, not the result of exciton capture or the energy release accompanying the luminescence. The barrier for thermally activated $B\rightarrow A$ return is $0.10\pm0.01$ eV, with no evidence of an intermediate configuration. Stress-induced splittings of the PL are satisfactorily analyzed as the sum of that for a highly localized hole plus that for a shallow Coulombically bound effective-mass electron. A tentative model is proposed involving a substitutional sulfur atom paired with an interstitial copper atom in two different nearby configurations. The low symmetry results from the tendency of the Cu interstitial to go off-center from the tetrahedral interstitial position. [S0163-1829(98)04636-0]

## I. INTRODUCTION

Strong photoluminescence (PL) at $\sim 1.3-1.4$ $\mu$m from thermally quenched sulfur-doped crystalline silicon was first reported by Brown and Hall in 1986.[1] The initial interest was technological as it was found that the luminescence was highly efficient at 77 K, and therefore could be of potential use in low temperature optoelectronic devices. Subsequently, however, the interest has turned to the physics of the defect responsible for the luminescence because of the discovery that it displays *metastability*, having two configurations in the lattice, each of which can be separately observed in the luminescence.

The chronological development leading up to our present understanding of this interesting system is as follows: Brown and Hall, in their first report,[1] concluded that the emission from the sulfur-doped material was from an exciton strongly bound to an isoelectronic trap as evidenced by a long radiative lifetime and a high thermal deactivation energy of $\sim 140$ meV. They suggested that sulfur was directly involved in the defect (a fact that has later been confirmed by the report of a very similar but distinctly different luminescence system in Se-doped silicon[2–4]). Beckett *et al.*[5] subsequently identified zero phonon lines (ZPL) from two distinct luminescence systems, labeled $A$ and $B$, each of which displayed two transitions, one forbidden but dominant at low temperatures (968.2 meV for $A$, 812.0 meV for $B$) and a second higher-energy one (977.0 meV for $A$, 821.9 meV for $B$), dominant at elevated temperatures ($T>15$ K). From far infrared absorption spectroscopy of the photopopulated excited state, they were able to show that the lowest excited state for each was composed of a deeply bound hole and an electron Coulombically bound by 65.3 meV for $A$ and 66.2 meV for $B$. Photoluminescence excitation spectroscopy (PLE) revealed several additional excited states. Of the excited states, three were tentatively interpreted as arising from within the $1S(A_1)$ electron effective-mass state and reflecting the $s=1/2$ electron and $j=3/2$ hole coupling scheme of Dean and Herbert.[6] Two additional higher-energy states were suggested to arise from the $1S(E)$ and $1S(T_2)$ states.

A subsequent study by Singh *et al.*[7] supplied evidence that the $A$ and $B$ systems arose from different configurations of the same defect, $A$ being the stable configuration, and $B$ a metastable one that is produced by the optical excitation at cryogenic temperatures. They showed also by Zeeman studies that the lowest-energy excited state for each configuration is a spin triplet ($S=1$) and that the next highest state (giving rise to the dominant ZPL at $T>15$ K) is a spin singlet ($S=0$). This revealed that, contrary to the original interpretation of Beckett *et al.*, the orbital angular momentum of the deeply bound hole is quenched, giving for it $s=1/2$. The origin of the additional excited states observed by Beckett *et al.* therefore remains presently unexplained. Henry *et al.*[8] studied further the conversion between the two configurations, making a rough estimate of $\sim 0.16$ eV for the thermal activation barrier for the $B$ to $A$ return conversion, but, in addition, concluding that a third configuration, not being seen in the luminescence, appeared to be required to interpret their results. Finally, a recent study of the photoexcitation energy dependence for the $A$ to $B$ conversion led to the proposal that the dominant conversion mechanism was excitonic Auger capture by the defect in an additional negative charged state of its $A$ configuration.[9]

There have been several ODMR studies reported for the triplet excited luminescent states of the two configurations.[10–13] No resolved hyperfine structure was observed in these conventional ODMR studies, but in a zero magnetic field study it was concluded that hyperfine interaction with a nuclear spin of $I=3/2$ could be detected, and the presence of a copper atom in the complex was proposed.[12] It was pointed out subsequently[14] that the distinctive phonon-assisted structure observed on the $A$ luminescence band is remarkably similar to that of another known copper-related band in silicon (ZPL at 1.0145 eV), supplying confirmation of their conclusion. In these ODMR studies, the symmetry of the $A$ configuration was concluded to be $C_{1h}$ (monoclinic $I$, containing a $\{110\}$ mirror symmetry plane), but the $B$ configuration was concluded to be $C_1$ (triclinic).

In the present paper, we describe PL and ODMR studies to probe further the structure and symmetry of the defect configurations and the mechanisms for conversion between the two. We arrive at conclusions that differ in several important respects from those cited above. In particular, we conclude that the symmetries of both $A$ and $B$ configurations are actually $C_1$ (triclinic), which, as reported earlier in a preliminary report,[14] we demonstrate unambiguously both by ODMR and a study of stress-induced splittings of the zero-phonon lines. Consistent with the conclusion of excitonic conversion, we supply direct evidence that the dominant conversion mechanism cannot be associated with the energy dumped into the defect local vibrational modes associated with the Stokes shift of the luminescence itself. However, we interpret our results to show that the dominant *below-band-gap* excitation mechanism is not excitonic capture, but rather requires direct optical excitation of the defect. We provide a precision determination of the thermal barrier for the $B$ to $A$ conversion and find no evidence of a third configuration. Finally, we attempt a model to explain the stress dependence of the PL spectra.

## II. EXPERIMENTAL PROCEDURE

Most of the samples studied were prepared by diffusion of sulfur at ~1050 °C into undoped high resistivity vacuum-floating zone silicon crystals in a sealed quartz ampoule for ~100−500 h. The solubility of sulfur at this temperature is approximately $2\times10^{15}$ cm$^{-3}$.[15] The visible surface damage was subsequently polished off and the samples etched with HF/HNO$_3$. For one set of experiments, similar samples were prepared from $p$-type vacuum floating zone silicon ($[B]\sim10^{16}$ cm$^{-3}$). For another set of photoluminescence studies, a sample produced by 200-keV ion implantation of sulfur, followed by a 30-min 1200 °C anneal was also used. In all cases, to produce the luminescence, the samples were reheated to ~700 °C for a few seconds and rapidly quenched into silicone oil or ethylene glycol.

The high resolution PL studies were carried out at King's College London. The conversion studies between the two configurations were performed using a custom-built drip-feed modification to an Oxford Instruments cryostat, with temperature regulation to ±0.1 K using an Oxford Instruments ITC-4 controller and a silicon diode sensor mounted in the sample holder. The actual sample temperature (±0.2 K) was measured by a calibrated Ge resistance thermometer (Lakeshore Cryogenics) mounted on the sample holder. The PL was excited using either the 514.5-nm line of an argon ion laser, the 1.064-$\mu$m or 1.319-$\mu$m line of a Nd YAG laser, or by a Burleigh color center laser tunable in the 1.47−1.73-$\mu$m range. The PL was dispersed using a 3/4-m single monochromator (Spex 1701), detected with a North Coast EO817S liquid-nitrogen-cooled germanium detector, and recovered using standard lock-in techniques. The uniaxial stress studies were performed at 4.2 K, with the samples immersed in liquid helium, or at 16 K in an Oxford Instruments helium flow cryostat. The PL was excited by the 514.5-nm line of an Ar$^+$ laser and the spectra were recorded using a Nicolet 60SX Fourier transform IR spectrometer, with a North Coast EO817S cooled germanium detector. Stress was applied along the long axis of x-ray oriented $12\times4\times2$ mm$^3$ samples, with long axes along $\langle100\rangle$, $\langle111\rangle$, or $\langle110\rangle$ directions. For the polarization studies, the samples were excited normal to the back $12\times4$-mm$^2$ surface and the PL was detected normal to the front $12\times4$-mm$^2$ surface. Luminescence emitted via the corners and edges was stopped by painting them with colloidal graphite.

The ODMR studies were performed at Lehigh University at pumped liquid helium temperatures (1.7 K) in an Oxford Instruments SM-4 superconducting magnet optical cryostat. The sample was mounted in a 35-GHz TE$_{011}$ cavity allowing for optical excitation and detection of the emitted light, and could be rotated to measure the angular dependence of the ODMR spectrum. A Gunn oscillator provided microwave power up to 70 mW, which was on-off modulated at ~500 Hz. Above-band-gap excitation at ~800−900 nm from a Ti-sapphire laser was used, and the luminescence was detected by a North Coast EO817S detector, with subsequent lock-in detection at the microwave modulation frequency. Similar to previously published results,[16] we encountered a strong nonresonant background signal with relatively fast decay, presumably arising from cyclotron resonance of the free carriers. It was eliminated using the method described by these authors of pulsing the excitation at twice the microwave modulation and lock-in detector frequency, and timing the detector to turn on after each fast carrier decay and off before the next laser pulse. Low-resolution PL studies were also performed in the ODMR cryostat using both Ti-sapphire and Nd YAG lasers for excitation.

## III. CONVERSION STUDIES

Shown in Fig. 1 are typical photoluminescence spectra under high resolution at 4.2 K, where only transitions from the lower triplet state of each are observed, labeled $^3S_A$ and $^3S_B$, and at ~15 K, where transitions from the higher lying-singlet state of each $^1S_A$ and $^1S_B$ begin to dominate. We will use this notation throughout this paper. (In earlier papers, before the triplet and singlet character of the excited states had been established, different, less meaningful labeling schemes have been used.)

Initially, upon cooling in the dark, only the $A$ luminescence bands appear. Under the photoexcitation used for the luminescence study, the $B$ luminescence grows in and the $A$ decreases. Under the proper conditions, which we will explore later in this section, almost complete conversion can occur. Upon subsequent annealing in the dark at ~40 K, the reverse $B\rightarrow A$ conversion occurs. In what follows, we will explore each of the two conversion processes.

### A. $B\rightarrow A$ Conversion

These studies were performed on an ion-implanted sample, the luminescence measurements being performed at

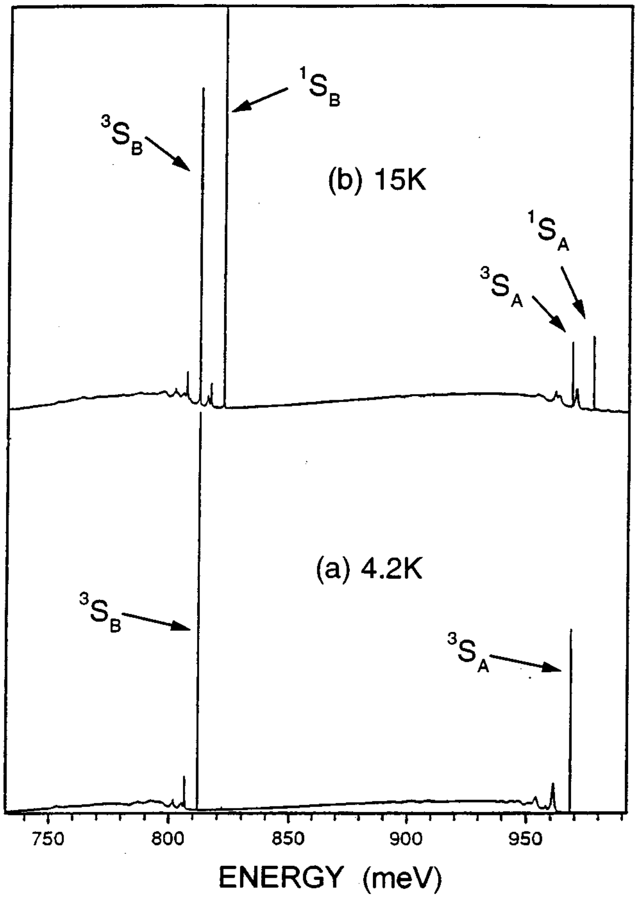

FIG. 1. High resolution PL spectra taken at (a) 4.2 K, and (b) 15 K of S-doped silicon following a rapid thermal quench from ~700 °C.

7 K using the 1.064-$\mu$m line of a Nd YAG laser as excitation. The samples were first converted to the $B$ configuration (~98% conversion after 5 min at 1-W excitation). They were then raised quickly to a fixed temperature, maintained there for a fixed period of time, cooled quickly again to 7 K, and the intensity of $^3S_A$ or $^3S_B$ was then recorded for 90 s under 10-mW laser excitation, by tuning the monochromator to the corresponding sharp zero phonon line (ZPL). By extrapolating the recorded intensity back to the start of the excitation, correction for any $A\rightarrow B$ conversion occurring during the monitoring was made. This procedure was repeated for both $^3S_A$ and $^3S_B$ at several time intervals for each annealing temperature, and at several temperatures.

At each temperature, the recovery was found to follow a simple exponential time dependence characteristic of first order kinetics, and in Fig. 2, we plot the experimentally determined time constants versus temperature. (The crosses result from PL measurements of the growth of $S_A$ taken *in situ* at the annealing temperature under weak excitation into the $^1S_B$ ZPL using the Burleigh color center laser. The $A\rightarrow B$ conversion was negligible under these excitation conditions and could be ignored; see the next section.) The results give an activation barrier of $0.10\pm0.01$ eV. As evident in the figure, the time constants for the recovery as measured separately for $A$ or $B$ are identical within the experimental accuracy. We see here, therefore, no evidence of a third, intermediate, configuration, as reported by Henry *et al.*[8]

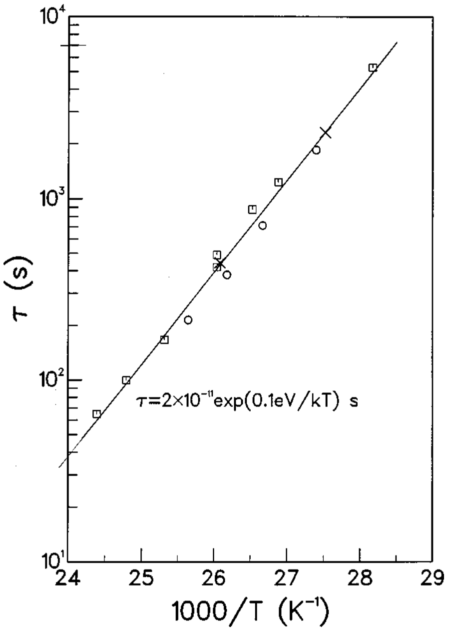

FIG. 2. Temperature dependence of the $B\rightarrow A$ recovery time constant, $\tau$, monitored by the intensity of the $^3S_A$ (circles), and $^3S_B$ (squares) luminescence at 7 K. The crosses indicate data monitored at the indicated temperature through $S_A$ while exciting into the $^1S_B$ ZPL.

With this additional information, we can summarize what is presently known concerning the electrical properties of the defect into a simple configurational coordinate (CC) diagram, as shown in Fig. 3. Contained therein for each configuration are the ZPL luminescence energy, the level position of the donor state above the valence band (the energy required to ionize the hole from the neutral state), and the

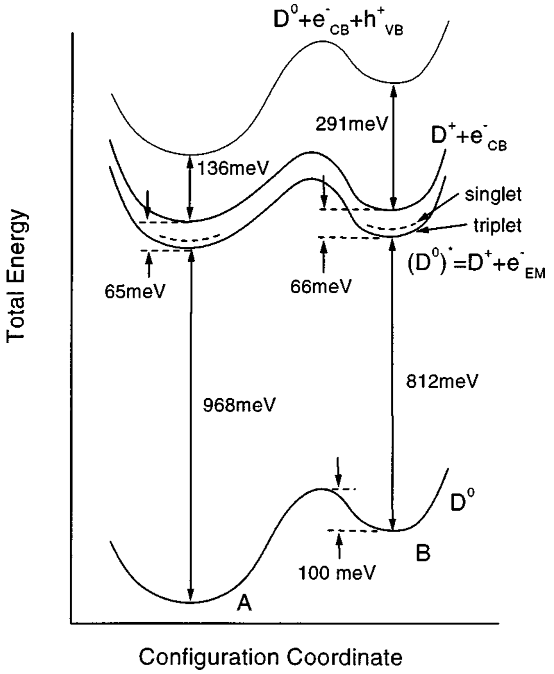

FIG. 3. Configurational coordinate diagram showing the two configurations of the S-related defect, their associated charge states, and level positions.

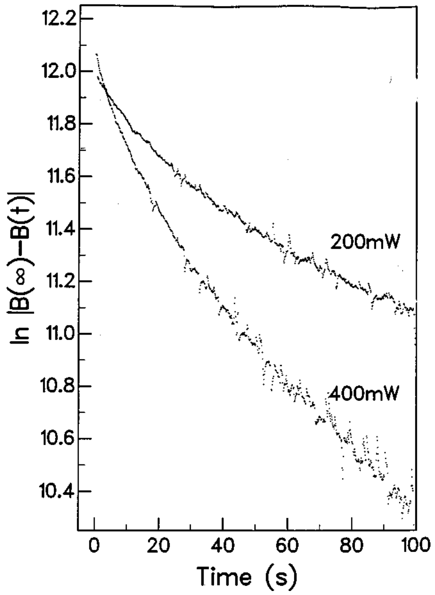

FIG. 4. Growth of $^3S_B$ luminescence under 1.064-$\mu$m excitation at T=7 K for two different excitation powers.

energy from the conduction band of the excited neutral state (the energy required to ionize the electron into the conduction band). In the ground neutral state, the barrier going from *B* to *A* is included, and the total energy of *A* has been placed lower than that of *B* to account for its greater stability. The only thing not known is how much lower *A* is than *B*, except that it must be $\gtrsim 0.03$ eV in order to account for the vanishing concentration of *B* when cooled in the dark from ~40 K (where it can still establish equilibrium). As drawn, the *A* configuration is still the stable one in the positive ionized state. That has not as yet been established, and we will attempt to explore that question later in this section.

### B. $A \rightarrow B$ Conversion

In Fig. 1, we note that, in addition to the sharp ZPL's, each has a broad phonon-assisted (Stokes) component to lower energies, the component for $S_A$ being somewhat greater, and extending to lower energies. This means that in the luminescence transition, energy is dumped into local lattice vibrations, which, from Fig. 1, could be for defect *A* as much as $\sim 0.1-0.2$ eV, but less for *B*.

Since the energy barrier for the thermally activated $B \rightarrow A$ return recovery is only 0.1 eV, one possible mechanism for the $A \rightarrow B$ conversion could be the luminescence itself. In this ''recombination-enhanced'' model, the local vibrational energy supplied by the Stokes transition would be sufficient to surmount the barrier, and the strong $A \rightarrow B$ preference could reflect the greater energy release efficiency for *A* versus *B*. We now test this attractively simple model.

We use the same setup as in the $B \rightarrow A$ conversion studies of the previous section, exciting the ion-implanted sample with the 1.064-$\mu$m Nd YAG laser line, partially defocused in an attempt at homogeneity over the sample, and recording the intensity versus time of the $^3S_A$ or $^3S_B$ ZPL through a monochromator. Before each run the sample was raised to ~65 K for 5 min and cooled in the dark to start from the same initial conditions. Shown in Fig. 4 is the conversion monitored by the growth of $^3S_B$ for two power levels. There is a definite departure from pure exponential behavior, but we assume in our analysis not greater than can be accounted for by unavoidable inhomogeneity in the excitation. We take the initial slope of each run as the measure of the conversion rate. In Fig. 5, we show the combined results of monitoring the growth of *B* and the decay of *A*. Within accuracy, the rate is linearly proportional to the excitation power over three decades. In addition, there is no significant difference between the results for *A* or *B*, as shown, again arguing against a third unseen intermediate configuration.

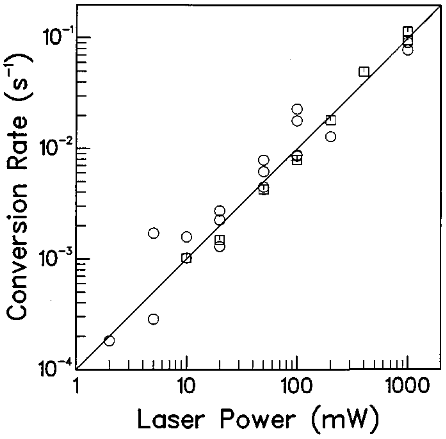

FIG. 5. $A \rightarrow B$ conversion rate at $T=7$ K vs power of 1.064-$\mu$m excitation, as monitored by the PL intensity of $^3S_A$ (circles) and $^3S_B$ (squares).

In Fig. 6, we show the intensity of the luminescence as monitored by the ZPL of each over the same range of excitation power. For *B*, the power dependence could be determined after first optically pumping all of the *A* centers to the *B* configuration. For *A*, the initial intensity was determined for each run by extrapolating back to the start of the excitation, to compensate for conversion occurring during the run. Here, it is clear that the luminescence is sublinear even at the lowest power level and saturates strongly at the higher excitation powers. Comparing this to the linear dependence of the conversion rate in Fig. 5, we can conclude immediately

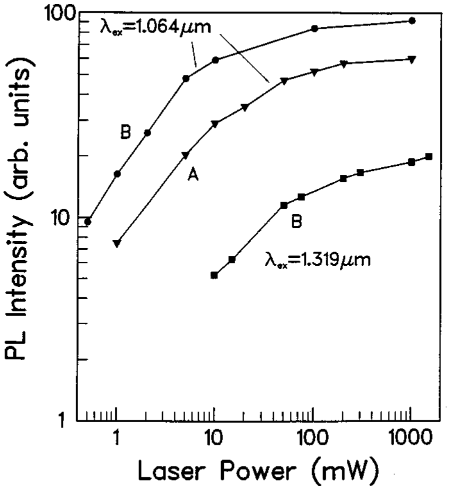

FIG. 6. PL intensity of $^3S_A$ and $^3S_B$ vs 1.064-$\mu$m excitation power.

that the luminescence itself does not provide a significant contribution to the $A \rightarrow B$ conversion, and a different mechanism must be involved.

In fact, a linear power dependence for the $A \rightarrow B$ conversion requires that the state from which the conversion process originates be constant in concentration over the full range of the excitation. This rules out, for example, *any* excitation-induced process from the excited state, because of its nonlinear occupancy dependence in Fig. 6. Instead, we are led, therefore, to the conclusion that the conversion process must be the result of excitation from a ground state of the $A$ defect, whose relative concentration is not significantly changed even at the highest excitation levels. This, in turn, implies that the luminescence saturation of Fig. 6 does not result from significant depopulation of the ground state.

Confirmation of this is seen in Fig. 6 where the ZPL PL intensity of $^3S_B$ versus 1.319 $\mu$m Nd YAG excitation power is also presented. We note the very similar saturation behavior as for the 1.064-$\mu$m excitation but saturating at a lower PL intensity. This suggests strongly that it is not saturation of the defect excited state that is occurring, but rather the limiting result of an indirect two-step excitation process of electrons and holes from unrelated deep level defects in the material. Luminescence will result from either sequential capture of the electrons and holes or capture of excitons formed from them. Evidence for such processes was previously noted by Beckett *et al.*,[5] who first observed both $S_A$ and $S_B$ luminescence with excitation energies well below the ZPL energies of either. As mentioned above, this is fully consistent with the linear dependence upon 1.064-$\mu$m excitation power, Fig. 6, which implies negligible depopulation of the appropriate defect ground state.

To probe this further, we have compared the conversion between above and below band-gap excitation on a diffused sample, for which the sulfur concentration should be relatively uniform throughout the bulk. These experiments were performed at Lehigh in the ODMR cryostat, the luminescence of the two bands being separated by interference filters (1250–1400 nm for $S_A$, 1500–1800 nm for $S_B$, with correction for the small overlap of the $S_A$ phonon-assisted tail into the range monitored for $S_B$), and recorded versus time. For the below-band-gap 1.064-$\mu$m excitation (1.165 eV, below the TA-assisted free exciton formation energy at 1.173 eV), which penetrates the sample, the conversion is similar to the studies described above, with almost complete conversion. For above-band-gap excitation (888 nm), however, the conversion is initially fast, but saturates quickly at only partial conversion, as shown in Fig. 7. Subsequent illumination from an unfiltered broad band xenon light source, with substantial below-band-gap contribution, completes the conversion, as shown.

These results further establish the independence of luminescence and conversion, but, in addition, present a strong argument that, for excitation below the phonon-assisted free exciton formation energy, direct *optical excitation* of the defect provides the dominant mechanism for conversion. When exciting above band gap, free carriers and excitons formed from them can diffuse beyond the optical penetration depth, producing the strong component of the observed luminescence that must come by their capture at defects farther into the bulk. But this capture is clearly highly ineffective in producing the conversion. We do not challenge the interpretation of Chen *et al.*[9] that the dominant mechanism could be an Auger process associated with exciton capture by an additional negative charge state of the defect $A$ configuration for excitations above the free exciton phonon-assisted formation energy. Their results, as well as those of Thewalt and Karasyuk[17] clearly demonstrate the sharp onset of a greatly increased conversion rate at this energy. (There are differences between finer, but important, details in the results and interpretations of the two groups, a subject of current controversy,[17–19] but the sharp onset upon free exciton formation is found by both.) Our results indicate, however, that, at least for excitation below this threshold, where the free exciton concentration is low, direct optical excitation becomes the dominant mechanism. In the figure, normalized intensities of both the $^3S_A$ and $^3S_B$ luminescence bands are plotted, as is their sum. Within accuracy, the sum remains constant throughout the transformation, again supplying no evidence of an invisible intermediate configuration.

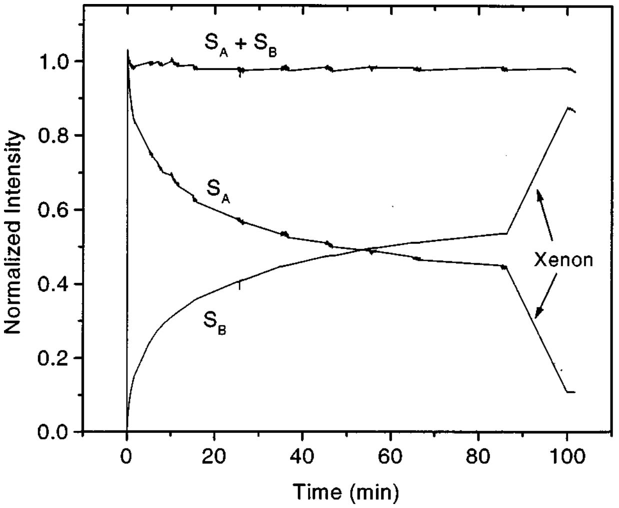

FIG. 7. $A$ and $B$ concentrations vs time in a S-diffused sample under 888-nm excitation at 4.2 K, as monitored by their normalized PL intensities. The last points result from broad band excitation with a xenon arc lamp source.

Although the saturation PL intensity in Fig. 6 for 1.319-$\mu$m excitation is only a factor of ~5 lower than that for the 1.064-$\mu$m excitation, we detect negligible $A \rightarrow B$ conversion rate at this lower energy, i.e., $\leqslant 2\%$ of that at the corresponding power for the 1.064-$\mu$m excitation. This suggests that the optical transition involved in the conversion is to a localized state of the defect in the conduction band, and it is its rapidly falling tail extending into the below-band-gap excitation energy region that is being excited. A similar effect has been reported for an optically induced reaction for the lattice vacancy in silicon, in that case, its migration.[20] The exact nature of the defect excited state cannot be determined, but such molecularlike states undoubtedly exist within the $d$ manifold of the copper atom, for example. An alternative possibility is a high vibrational state of the $B$ configuration, which on the CC diagram of Fig. 3 would be the harmonic extension of the excited $B$ state curve past the $A$-$B$ barrier (resulting from the ‘‘anticrossing’’ with the corresponding harmonic extension of the $A$ excited-state curve) toward the $A$ equilibrium coordinate, allowing a direct transition to the $B$ configuration.

### C. Bistability or metastability?

As mentioned above, none of the available information so far tells us which of the two configurations is the stable one in the positive, or, what is equivalent, the excited neutral state of the defect. In Fig. 3, the CC curves have arbitrarily been drawn so that the *A* configuration remains the stable one, but that has not been established. In fact, the 156-meV difference between the *B* and *A* luminescence energies means that the energy difference between *A* and *B* configurations in the positive charge state is reduced by that amount from that in the neutral charge state, making it quite possible that the *B* configuration becomes the stable one there. If so, the defect is *bistable,* joining the ranks of a growing number of defects with that interesting property.[21]

To explore this question, we have attempted to produce the center in *p*-type material, to determine which configuration is initially observed by PL in that material after cooling in the dark. Following the same *S* diffusion and reheat-quench procedures that were successful in the undoped silicon, we found it very difficult to produce the luminescence in *p*-type material ($[B]\sim 10^{16}$ $\mathrm{cm}^{-3}$). After several attempts, only one of the samples contained the luminescence. For it, again only the *A* luminescence was present after initial cooldown. Using a four-point probe at room temperature, this sample still has low resistivity, and presumably is therefore still *p*-type, after the diffusion, but had high resistivity after the reheat and quench to activate the centers. The Fermi level may therefore not have remained close enough to the valence band to produce the positive charge state, and the initial absence of the *B* configuration in this sample may simply reflect that failure.

Our results therefore remain inconclusive on this important question. The apparent difficulty in producing the defect in *p*-type material could be a real limitation, reflecting the effect of the charge states of the individual constituents upon their ability to react. If so, a more clever experiment will have to be devised to answer this question.

## IV. ODMR RESULTS

### A. Spectra

The saturation of conversion using above-band-gap excitation shown in Fig. 7 is very convenient because it makes possible the prolonged illumination times required for ODMR studies of the $^3S_A$ system, which would otherwise rapidly disappear. As a result the ODMR experiments described below were performed on *S*-diffused samples using 880-nm excitation from a Ti-sapphire laser, where the two luminescence contributions persisted essentially indefinitely and were comparable.

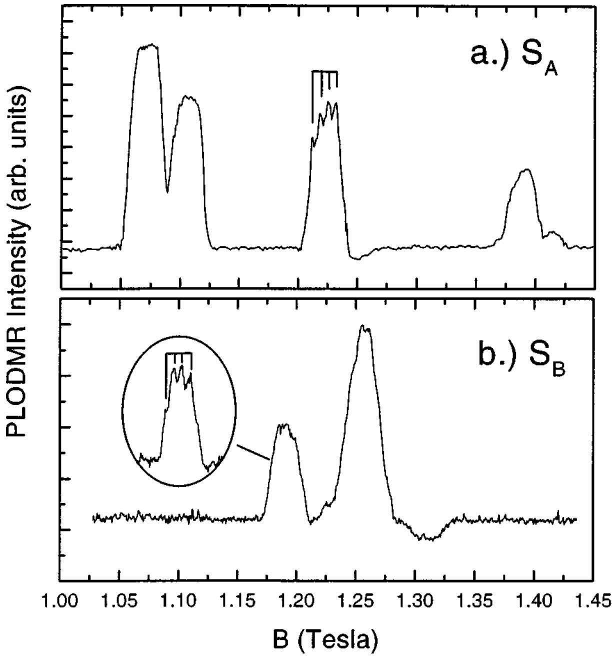

FIG. 8. ODMR spectra at 1.7 K, with $\mathbf{B}\|[111]$, observed in the (a) $^3S_A$ and (b) $^3S_B$ PL spectra taken at 1.7 K using 35 mW of 769-nm excitation from a Ti-sapphire laser. The inset in (b) was taken at $\mathbf{B}\|[111]+2.5°$ ($\Psi=57.2°$, see Fig. 11).

Figure 8 shows the ODMR spectra observed in the $^3S_A$ and $^3S_B$ bands at 1.7 K with the magnetic field (**B**) oriented along a crystal $\langle 111\rangle$ direction. Here, as in the experiments described above, optical interference filters were used to separate the bands (1250–1400 nm for $^3S_A$, 1500–1800 nm for $^3S_B$), but capture most of the luminescence intensity of each. All of the ODMR signals show a broad flat-topped shape suggesting the presence of an unresolved hyperfine interaction with a single nucleus. As seen in the figure under higher resolution, one of the lines for each spectrum shows four partially resolved lines, not previously reported. These results provide, therefore, direct confirmation that a 100% abundant spin $I=3/2$ nucleus is indeed involved, consistent with the evidence presented previously from ODMR studies in zero magnetic field.[12]

Shown in Figs. 9 and 10 are the angular dependences for the $^3S_A$ and $^3S_B$ ODMR spectra, respectively. The solid lines in the figures represent the best fit to the data using a Hamiltonian of the form

$$\mathcal{H}=\mu_B\mathbf{S}\cdot\mathbf{g}\cdot\mathbf{B}+\mathbf{S}\cdot\mathbf{D}\cdot\mathbf{S}+\mathbf{I}\cdot\mathbf{A}\cdot\mathbf{S} \tag{1}$$

with electronic and nuclear spins of $S=1$ and $I=3/2$, and the parameters given in Table I. For the fit, the principal axes of **g** and **D** were constrained to be the same, and the principal values of **D** were further taken to be those determined rela-

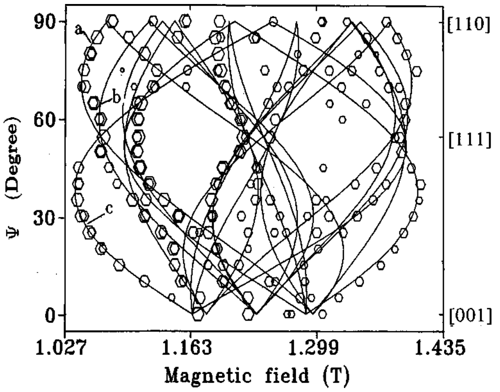

FIG. 9. Angular dependence of the $^3S_A$ ODMR spectrum at 1.7 K using 811-nm excitation from a Ti-sapphire laser. The Hamiltonian parameters used to generate the solid line fit are given in Table I.

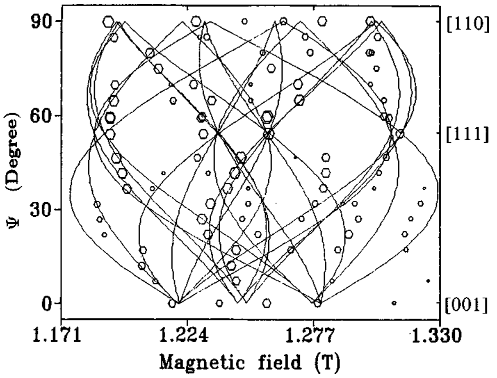

FIG. 10. Angular dependence of the $^3S_B$ ODMR spectrum at 1.7 K using 811 nm excitation from a Ti-sapphire laser. The Hamiltonian parameters used to generate the solid line fit are given in Table I.

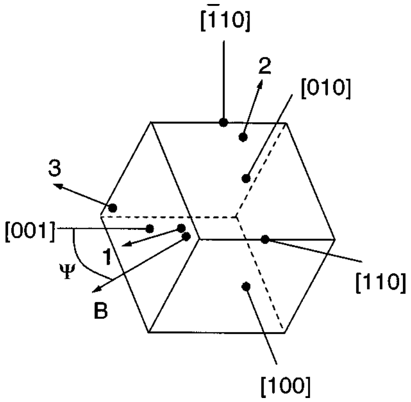

FIG. 11. Diagram illustrating the directions of the principal axes of **g** and **D** for a representative orientation of the $^3S_A$ or $^3S_B$ defect and the $(\bar{1}10)$ plane of rotation for the magnetic field.

tively precisely in the previous zero-field experiments.[12] (Such zero field experiments provide no information concerning the *orientation* of the principal axes of **D**, and hence the defect symmetry.) The principal axes determined here share angles with a set of cubic axes of the crystal whose cosines are listed in Table I. The directions of these axes for a representative defect orientation with respect to the cubic crystal axes are shown in Fig. 11.

Consistent with previous published analyses for both centers, the projection of the principal $D_1$ axis onto the $(\bar{1}10)$ plane is ~17° away from the [111] direction, but our results reveal that, for $^3S_A$, it is also tilted out of the plane by $\pm 7°$. The angular dependence shows three distinct branches that superpose only for $\mathbf{B} \| [111]$ ($a$, $b$, and $c$ in Fig. 9, arising from the three sets that are tilted 17° from their common [111] direction). For $C_{1h}$ symmetry, branches $a$ and $b$ would superpose throughout the complete angular dependence. The fact that they split apart determines the symmetry to be $C_1$ (triclinic), not $C_{1h}$, as concluded previously.[13] In the next section, we rule out the possibility that the $a$-$b$ splitting could have resulted from an accidental tilt of the sample in mounting (i.e., the $[\bar{1}10]$ crystal axis misaligned from the vertical axis of rotation).

Our results for $^3S_B$ are less accurate due to the poor resolution of the spectra. However, they agree with those of Chen *et al.*[13] in that we find the 1 axis within ~1° of the $(\bar{1}10)$ plane, but find the 2 axis tilted from the $[\bar{1}10]$ by ~18°, compared to their value of ~38°. We both agree, however, that its symmetry is $C_1$ (triclinic), and much of the discrepancy between the two results can possibly be explained from the poor resolution in both our and their spectra.

### B. Polarization properties

Shown in Fig. 12 is the $^3S_A$ ODMR spectrum at three different magnetic field orientations with a linear polarizer (Polaroid HR) inserted in the path of the luminescence. The axis of the polaroid is either parallel (vertical) or perpendicular (horizontal) to the $[\bar{1}10]$ direction around which the sample is rotated, as shown in Fig. 11. The signals have been normalized by dividing by the total PL intensity in each case, to correct for the different internal reflection coefficients for the two polarizations.

The positions for the low field transitions of the three inequivalent sets of orientations discussed above ($a$, $b$, and $c$ of Fig. 9) are indicated in Fig. 12. Strong polarization effects are clearly observed, orientation $a$ being polarized strongly horizontal, $b$, strongly vertical, and $c$, weakly horizontal. The ODMR spectra for $^3S_B$ also exhibit large polarization effects. This observation of distinctly different polarization properties associated with the $a$, $b$, and $c$ branches provides the required and unambiguous proof that they do indeed derive from three inequivalent orientations, and that the splitting between $a$ and $b$ does not result from a crystal tilt.

These results have another important consequence. The fact that the ODMR signals from different defect orientations display different polarization properties provides unambigu-

TABLE I. Spin Hamiltonian parameters for the defect orientation illustrated in Fig. 11, and used for the fits to the $^3S_A$ and $^3S_B$ ODMR spectra.

| Spectrum | $g$ | $D$ (MHz) | $n[100]$ | $n[010]$ | $n[001]$ | $\lvert A\rvert$ (MHz) |
|---|---|---|---|---|---|---|
| $^3S_A$ | $g_1=2.055$ | $D_1=3610$ | +0.780 | +0.353 | +0.517 | ~200(10) |
| | $g_2=2.015$ | $D_2=-700$ | −0.174 | −0.174 | +0.721 | |
| | $g_3=2.022$ | $D_3=-2900$ | +0.602 | +0.602 | −0.462 | |
| $^3S_B$ | $g_1=2.008$ | $D_1=1470$ | +0.814 | +0.421 | +0.400 | ~180(10) |
| | $g_2=2.018$ | $D_2=-180$ | −0.168 | −0.489 | +0.865 | |
| | $g_3=2.015$ | $D_3=-1290$ | +0.557 | −0.763 | −0.327 | |

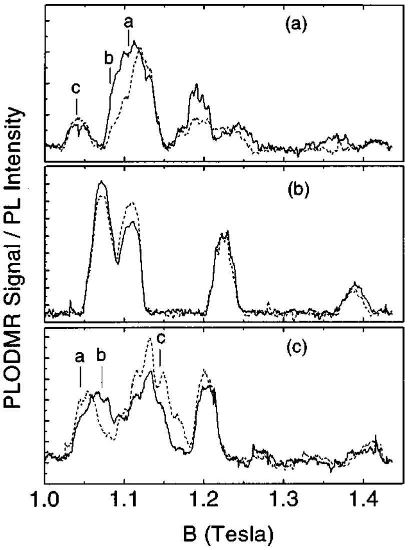

FIG. 12. Dependence of the ${}^3S_A$ ODMR intensities on the linear polarization of the luminescence (solid, $\mathbf{E}\parallel[\bar{1}10]$; dashed, $\mathbf{E}\perp[\bar{1}10]$) for (a) $\Psi=42.7°$, (b) $\mathbf{B}\parallel[111]$, $\Psi=54.7°$, and (c) $\Psi=72.7°$. The positions of the three branches labeled $a$, $b$, and $c$ in Fig. 9 are indicated.

ous proof that the *defect being studied by the ODMR is indeed the defect producing the luminescenc*e, and not indirectly involved. In ODMR studies, this issue is always one of concern, and one that can only be directly addressed in this manner.

Such studies on a well-resolved spectrum at several magnetic field and optical collection directions could potentially be used to make an accurate determination of the optical dipole direction for the transition with respect to the defect axes, another important bit of information concerning the defect. It would be extremely difficult here, however, because of the poor resolution in the spectrum, and it was not attempted. However, the results for the *a*, *b*, and *c* orientations in Fig. 12 by themselves provide some information for ${}^3S_A$ in this regard. Their polarization properties can be matched reasonably well assuming the dipole moment direction to be primarily in the 2-3 plane, approximately 55° from the +2 axis and 35° from the +3 axis. (The light was collected from the [110] surface of the crystal, and in analyzing the polarization properties, proper correction for refraction at the surface was necessary to obtain the correct *internal* perpendicular polarization directions.)

Careful studies of the $A$ and $B$ ODMR intensities versus time during the above- and below-band-gap conversion studies described earlier in Sec. III B were also performed. Within accuracy, they followed their corresponding luminescence band intensities, consistent again with the conclusion above from the polarization studies that the ODMR is, in each case, from the same defect that produces the luminescence.

## V. UNIAXIAL STRESS STUDIES OF THE ZPL'S

In Figs. 13 and 14, we show the splittings produced by uniaxial stress along three different crystal directions for the singlet and triplet ZPL transitions of $A$ and $B$, respectively. In all four cases, the splitting into 3, 4, and 6 lines for the $\langle 100\rangle$, $\langle 111\rangle$, and $\langle 110\rangle$ stress directions, respectively, uniquely determines the symmetry to be triclinic ($C_1$).[22] Some of the splittings are small and in an earlier publication we concluded that they could be spurious, arriving at the conclusion of higher symmetry in each case.[23] However, following up on the lower symmetry conclusions from the ODMR studies, we have carefully repeated the stress experiments, and extended them to higher stresses. From these studies, it is now clear that the splittings are genuine, the several lines in each case arising from the number of inequivalent sets of defect orientations with respect to the applied stress direction. Each component is observed to have different polarization properties,[14] as illustrated in Fig. 15.

### A. Model for analysis

As summarized in Fig. 3, the excited emitting state arises from the triplet or singlet combination of a loosely bound effective-mass-like (EM) $s=1/2$ electron with a deeply bound (136 meV for $A$, 291 meV for $B$) $s=1/2$ hole. We model the response to stress, therefore, as that of the sum of the contributions of the two weakly coupled individual particles. Consistent with this, we note that the splittings observed for the triplet and singlet states of each system are almost identical. In what follows, we will therefore concentrate our analysis on the ${}^3S_A$ and ${}^3S_B$ results only.

For the deeply bound hole, we utilize the generalized treatment of Kaplyanskii,[22] where the change in energy of a particular defect orientation in a cubic crystal can be expressed as

$$\delta E=A_1\sigma_{xx}+A_2\sigma_{yy}+A_3\sigma_{yy}+A_4\sigma_{xy}+A_5\sigma_{yz}+A_6\sigma_{zx}, \qquad (2)$$

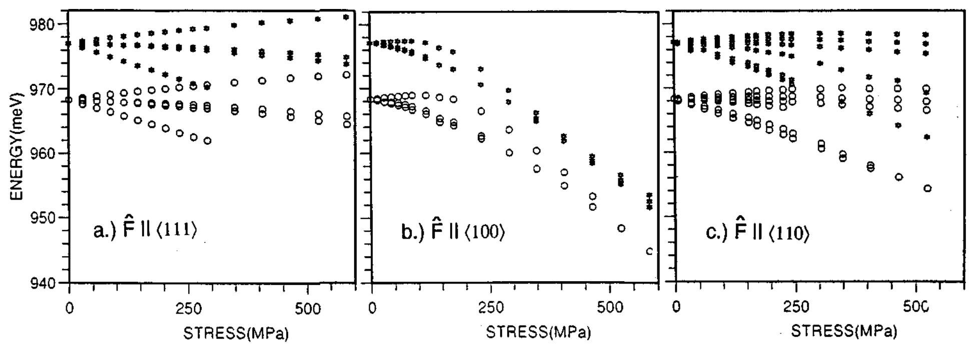

FIG. 13. Splitting of the $S_A$ PL ZPL's under (a) $\langle 111\rangle$, (b) $\langle 100\rangle$, and (c) $\langle 110\rangle$ stress at ~14 K.

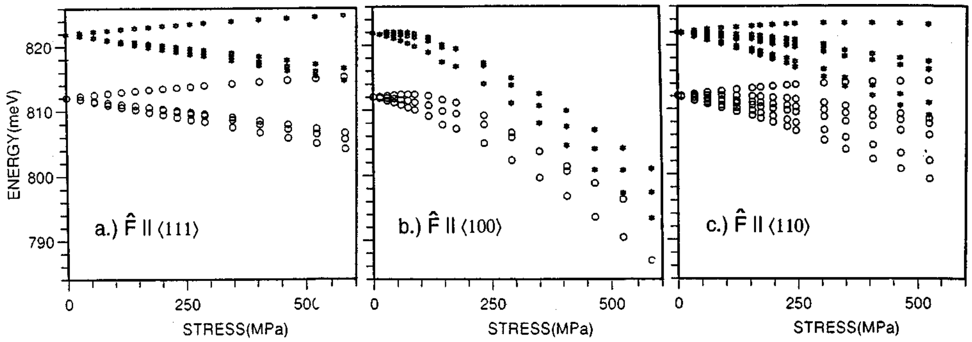

FIG. 14. Splitting of the $S_B$ PL ZPL's under (a) ⟨111⟩, (b) ⟨100⟩, and (c) ⟨110⟩ stress at ~14 K.

where the $A_i$ form the elements of a piezospectroscopic tensor, which describe the linear shifts versus stress, and the $\sigma_{ij}$ are the elements of the symmetric stress tensor resolved along a set of cubic $x=[100]'$, $y=[010]'$, $z=[001]'$ axes, defined for that defect. (At this point there is no established relationship between the cubic axes defined for a specific defect orientation detected in the ODMR spectra, Fig. 11, and those for the optical stress splittings defined here, or for the four choices of defect orientation for each of the six sets of permuted axes.) For a defect of $C_1$ symmetry, all six components of $A_i$ are required, which can be uniquely determined using Table III of Ref. 22 from the splittings produced by stress along the ⟨100⟩, ⟨111⟩, and ⟨110⟩ directions.

For the electron, we follow the simple deformation potential treatment developed for the EM shallow donor in silicon,[24] where, in cubic symmetry, the sixfold degeneracy of the ⟨100⟩ conduction-band valleys causes the ground 1$S$ hydrogenic state to split into three distinct energy states given by a 1$S$ modulating envelope function times the following linear combinations of the valleys:

$$\begin{aligned}
&\text{singlet } A_1=(1/\sqrt{6})(1,1,1,1,1,1),\\
&\text{doublet } E_\theta=(1/\sqrt{12})(2,2,-1,-1,-1,-1),\\
&E_\epsilon=(1/2)(0,0,1,1,-1,-1),\\
&\text{triplet } T_{2x}=(1/\sqrt{2})(1,-1,0,0,0,0),\\
&T_{2y}=(1/\sqrt{2})(0,0,1,-1,0,0),\\
&T_{2z}=(1/\sqrt{2})(0,0,0,0,1,-1),
\end{aligned} \tag{3}$$

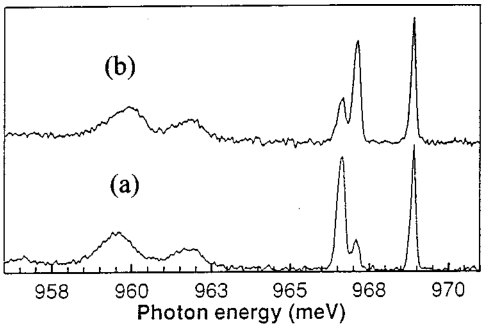

FIG. 15. Polarization dependence of the $^3S_A$ ZPL's under 98 MPa [001] stress at 4.2 K. (a) $\mathbf{E}\parallel[001]$; (b) $\mathbf{E}\perp[001]$.

where the 6-component vector notation denotes the coefficient of the valley oriented along the $k_{100}$, $-k_{100}$, $k_{010}$, $-k_{010}$, $k_{001}$, and $-k_{001}$ directions, respectively. The energy shift of the $j$th valley, with respect to the center of gravity for all of the valleys, under applied stress of magnitude $T$ (positive for tension) can be written as

$$\delta E_j=\Xi_u T(s_{11}-s_{12})[(\hat{\mathbf{k}}_j\cdot\hat{\mathbf{F}})^2-\tfrac{1}{3}], \tag{4}$$

where $\hat{\mathbf{k}}_j$ is a unit vector along the ⟨100⟩ direction of the $j$th valley in $k$ space, $\hat{\mathbf{F}}$ is a unit vector parallel to the applied stress in real space, $\Xi_u$ is the shear deformation potential (8.77 eV for the free electron), and $s_{11}$ and $s_{12}$ are elastic moduli of the crystal. This causes linear splittings within the $T_2$ and $E$ states versus applied stress along a cube axis, but also introduces off-diagonal coupling between the $A_1$ and $E$ states, with corresponding nonlinear effects for them.

In the analysis, we will consider two distinct models. In the first model, we assume the $A_1$ EM state for the electron to be lowest in energy, as is the usual case due to the Coulomb attractive central cell effect, which in this case arises from the positive bound hole. In the second model, we take the $E$ state lowest. The rationale for this second choice is twofold: (1) the 65–66 meV binding is larger than that for the usual neutral chemical donors, and (2) the presence of copper in the core of the defect could supply an empty localized $d$ state of $e$ symmetry that, by mixing with the EM electron $E$ state, might lower it preferentially. In each case, we will allow an internal stress resulting from the low symmetry of the defect core to split the EM states in the absence of externally applied stress.

In either model, the electron experiences no splittings from ⟨111⟩ stress, so that values for $A_4$, $A_5$, and $A_6$ are immediately determined from the ⟨111⟩ results. In addition, including, for convenience, the hydrostatic component for the electron into that for the hole, the sum $(A_1+A_2+A_3)/3$ is also determined. The values for these parameters, determined from the initial low stress slopes, are included in Table II, and the corresponding match to the ⟨111⟩ stress results for $^3S_A$ is given in Figs. 16 and 18. We note a small additional quadratic term emerging at high stresses, the origin of which could presumably come from either the electron or the hole, but which we will ignore in the following analysis. For the ⟨100⟩ and ⟨110⟩ stress results, we must include the contribution from the electron, which differs for the two models.

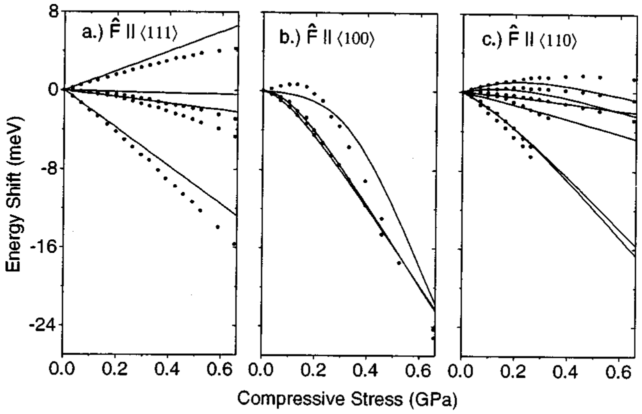

FIG. 16. Theoretical fits to the $^3S_A$ stress splittings using model I ($A_1$ ground state) for (a) ⟨111⟩, (b) ⟨100⟩, and (c) ⟨110⟩ stress and the parameters of Table II.

### 1. $A_1$ state lowest

In Fig. 16, we include a match to the $^3S_A$ stress results, assuming the $A_1$ EM state to be lowest, $6\Delta_c$ below the $E$ state in the absence of internal or external stresses. The $A_i$ parameters for the hole, and the various parameters for the EM electron are included in Table II. (The specific assignment of the three ⟨111⟩ stress-determined values to $A_4$, $A_5$, and $A_6$ has been made for the best fit to the ⟨110⟩ stress results, which by containing both $\sigma_{ii}$ and $\sigma_{ij}$ stress components, serves to establish the same set of defect axes for all six components.) Internal stresses $\sigma_{ii0}$ have been included along the $x$, $y$, $z$ cubic axes of the defect, which serve to shift and split the EM states in the absence of externally applied stress, as shown in Fig. 17. Here we see that the presence of an internal $\sigma_{zz0}$ tensile stress causes an externally applied $[001]'$ compressive stress [the prime denotes that it is along the $z$ axis defined by Eq. (2) for the defect] to first reduce the total stress along that direction providing an initial small positive slope for the $A_1$ ground-state energy, which increases to a maximum when the total $[001]'$ stress is zero, and then decreases. This has been necessary in order to try to match the behavior for the upper branch of Fig. 16(b). The smaller internal stresses $\sigma_{xx0}=-\sigma_{yy0}$ serve to produce the crossover in the two lower branches. The value of $\Xi_u$ for best fit is reduced somewhat from the free electron value (8.77 eV), but this is not inconsistent with similar reductions observed for the deeper, and hence more localized, chemical donor states.[25]

TABLE II. Hole and electron parameters for the fits to the $^3S_A$ and $^3S_B$ stress results. (I) or (II) denotes the model with the EM $A_1$ or $E$ state assumed lowest, respectively.

| Parameter | $^3S_A$(I) | $^3S_A$(II) | $^3S_B$(I) | $^3S_B$(II) |
|---|---|---|---|---|
| $A_1$(meV/GPa) | 6.5 | 5.0 | 11.0 | 4.0 |
| $A_2$ | 4.5 | 1.0 | −1.0 | −1.0 |
| $A_3$ | −21.0 | −16.0 | −24.0 | −17.0 |
| $A_4$ | −2.0 | 12.3 | 6.2 | 4.5 |
| $A_5$ | 12.3 | −2.0 | 7.8 | 6.2 |
| $A_6$ | 10.2 | 10.2 | 4.5 | 7.8 |
| $\frac{1}{3}(A_1+A_2+A_3)$ | −3.3 | −3.3 | −4.7 | −4.7 |
| $6\Delta_c$(meV) | 14.0 | −30.0 | 15.0 | −30.0 |
| $\Xi_u$(eV) | 7.3 | 7.0 | 7.3 | 6.5 |
| $\sigma_{xx0}$(GPa) | 0.008 | 0.015 | 0 | −0.022 |
| $\sigma_{yy0}$(GPa) | −0.008 | −0.015 | 0 | +0.022 |
| $\sigma_{zz0}$(GPa) | −0.265 | −0.170 | −0.245 | −0.165 |

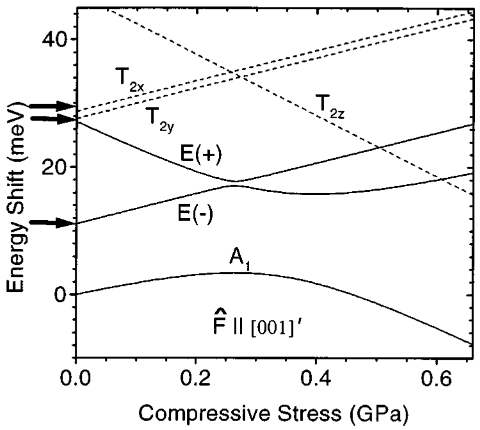

FIG. 17. Calculated energies for the $^3S_A$ bound electron $1S$ manifold for model I ($A_1$ state lowest) under externally applied compressive stress along the defect $[001]'$ axis. The parameters used for the calculation are those of Table II that were determined from the fit shown in Fig. 16. Shown by arrows are the relative positions of the additional excited states inferred from the PLE studies.

Although the general features of the ⟨100⟩ stress results are reproduced, the fit is not really satisfactory; the positive increase before turnaround in the upper branch at low stresses substantially exceeds the theoretical fit. The results for the fit to $^3S_B$ data, not shown, suffer the same difficulty. To better match the ⟨100⟩ results, we now consider the second model.

### 2. E state lowest

In Fig. 18, we show the best fit we have obtained for the $^3S_A$ stress results starting from the assumption that the EM electron $E$ state is lowest. The various fitting parameters are also given in Table II. In Fig. 19, the $1S$ EM states, as split by the built-in stresses, are shown again versus stress along the defect $[001]'$ axis. Here, we see that a substantially

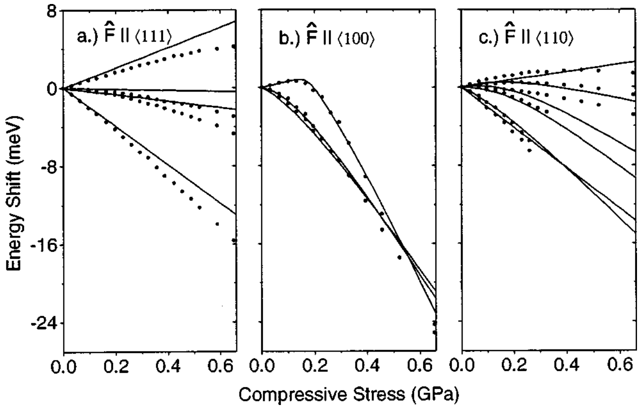

FIG. 18. Theoretical fits to the $^3S_A$ stress splittings using model II ($E$ ground state) for (a) ⟨111⟩, (b) ⟨100⟩, and (c) ⟨110⟩ stress and the parameters of Table II.

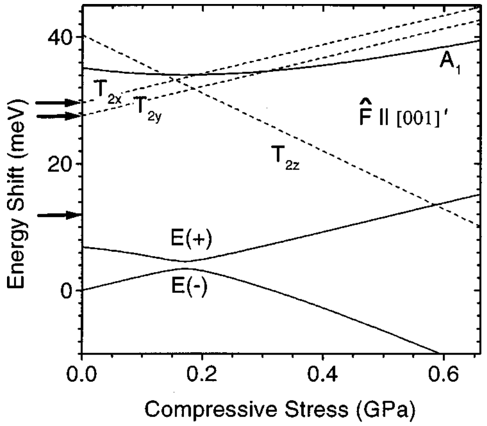

FIG. 19. Calculated energies for the $^3S_A$ bound electron 1$S$ manifold for model II ($E$ state lowest) under externally applied compressive stress along the defect $[001]'$ axis. The parameters used for the calculation are those of Table II that were determined from the fit shown in Fig. 16. Shown by the arrows are the relative positions of the additional excited states inferred from the PLE studies.

greater initial rise and curvature for the lowest-energy state under $[001]'$ applied stress now can arise from a level anticrossing of the $e$ states as the internal $\sigma_{zz0}$ is canceled by the applied stress. Again, a small $\sigma_{xx0}=-\sigma_{yy0}$ has been introduced, in this case adjusted to supply the degree of anticrossing level repulsion required to match the curvature of the upper branch of Fig. 18(b) in detail.

As seen in the figure, this greatly improves the fit. A similar improvement occurs for the $^3S_B$ results.

### *3. Comparison to the ODMR symmetry determination*

Except for agreement now on the symmetry classification of the two configurations, there is no direct connection between the orientation of the principal axes of the ODMR spectra given in Fig. 11, and the axes determined from the various branches of the stress-split optical spectra as defined by the piezospectroscopic tensor **A**. For a low symmetry $C_1$ center, the same number of distinct branches must occur in the optical stress results for the various stress directions as in the ODMR spectra with the magnetic field **B** oriented along the corresponding direction. This is because, by symmetry, they each correspond to the same set of orientations that are equivalent with respect to the orientation of the applied perturbation. So there is no clue there. The necessary information could only come from detailed correlation of the optical polarization properties of each. Comparing the polarization properties described for the ODMR spectra in Sec. IV B with those evident in Fig. 15, for which the optical viewing directions are closely similar, suggests that the individual three split lines of increasing energy in the optical studies could correspond to the defect orientations labeled $a$, $b$, $c$, respectively in the ODMR studies. If so, the piezospectroscopic tensor $[100]'$,$[010]'$,$[001]'$ axes of Eq. (2) would correspond to the [100], [010], [001] axes, respectively, of the specific defect orientation shown in Fig. 11. This would mean that the principal internal strain component $\sigma_{zz0}$ is along the [001] axis for the defect orientation shown in Fig. 11. However, *this identification must be considered tentative* for several reasons. We have already mentioned the difficulty of polarization studies of the ODMR transitions. In addition, in the optical studies there is evidence of changes in the polarization properties versus stress making it possibly unreliable to attempt correlation with the ODMR results, which are obtained at zero stress.

### *4. Comparison to PLE spectroscopy*

The photoluminescence excitation spectroscopy studies of Beckett *et al.*[5] detected several higher lying excited spin singlet states for both the $A$ and $B$ configurations. For the $A$ configuration, they were estimated to be at 11.0, 27.7, and 29.5 meV above the lowest-energy singlet state, for $B$, they were 11.9, 26.4, and 29.6 meV. We here investigate the two models above to see if either or both can supply an identification of these states as arising from the other EM states within the 1$S$ manifold for the excited singlet state. We expect the relative positions of these states to be similar to those within the triplet spin state, as given therefore in Figs. 17 and 19, at zero external stress. To aid this comparison, we have noted by arrows the positions of these PLE-determined excited-state levels with respect to the lowest EM state at zero external stress in the figures.

Consider model I ($A_1$ state lowest), as shown in Fig. 17. The fit to the stress-splitting data turns out to be relatively insensitive to minor adjustments of the value of $6\Delta_c$. (A satisfactory match was initially obtained with a value of 24 meV, with slight adjustment of the other parameters to compensate.)[26] As a result, in deriving the specific parameters given in Table II, it was possible to further restrict the $A_1$ to lower $E$-level splitting at zero applied stress to match the 11.0-meV PLE excitation energy, as shown in the figure, still with a satisfactory fit. This, in turn, automatically places the upper $E$ state close to the 27.7-meV PLE excitation energy. Finally, since the placement of the center of gravity for the $T_2$ states is arbitrary in our analysis, we have, in the figure, placed it so that the $T_{2x,y}$ states end up also in the region of the 27.7- and 29.5-meV excitations. A logic for this placement is that, in so doing, the $T_2$ center of gravity is $\sim$35 meV above the ground $A_1$ state, ending up therefore close to the expected EM binding energy value of $\sim$30 meV. Alternatively, we might have chosen a lower center of gravity for the $T_2$ states so that the $T_{2z}$ state matched the 29.5-meV level. In any event, it appears that model I has sufficient flexibility to satisfactorily accommodate the PLE excitation results. Very similar results are found for the model I match to the $^3S_B$ results.

However, in the case of model II, Fig. 19, accounting for the PLE excitations is somewhat less satisfactory. On the positive side, the $\sigma_{xx0}$ and $\sigma_{yy0}$ components required to match the curvature of the upper branch of the $\langle 100\rangle$ stress results provide splittings between the $T_{2x}$ and $T_{2y}$ states, which match closely for both $^3S_A$ and $^3S_B$ the splittings between the two higher-energy states seen in the PLE. The center of gravity for the $T_2$ states has therefore been selected to make this obvious match in Fig. 19. In so doing, its center of gravity again lies close to the expected EM value, as might reasonably be expected. However, the model leaves little flexibility in the position of the E(+) level, and it does not appear possible to raise it sufficiently to satisfactorily match the first PLE level and still match the $\langle 100\rangle$ stress results for either ${}^3S_A$ or ${}^3S_B$.

Another possibility for an energy-level crossing is if the $T_2$ state were lowest. It is possible, of course, that the unoccupied copper $d$ orbital is of $t_2$ symmetry, making $T_2$ the lowest 1$S$ EM state. However, in that case, the level crossing would be a true crossing, giving a sharp, not rounded, slope change to the upper transition in the $\langle 100\rangle$ stress results, since Eq. (4) provides no off-diagonal coupling between the $T_2$ states or from them to the other states. Therefore, we have not considered this possibility further.

And so, we are faced with a dilemma. The model with the $E$ state lowest fits the stress data extremely well. It does not appear, however, to supply a simple direct explanation of the first excited PLE state. The model with the $A_1$ state lowest appears incapable of a good match to the stress results, but is potentially capable of accounting for the PLE states. In order to more properly identify the parentage of the PLE states, it would be highly desirable to study the effects of applied uniaxial stress on the PLE spectrum, as has successfully been done via absorption studies in the case of a different neutral donor luminescent system,[27] and used to unravel its excited EM structure.[28] In the absence of such results, however, we must accept the present uncertainty. We recognize that there remains flexibility in the positioning of the $T_2$ levels to account for some of the PLE levels, and, of course, we cannot rule out the possibility that low-lying excited levels for the bound hole play a role. Evidence for this might be cited in the nonlinear effects evident in Figs. 16(a) and 18(a), which are not accounted for in the EM approximation.

## VI. SUMMARY AND CONCLUSIONS

We have established the following concerning this much studied metastable PL system in S-doped silicon.

(1) The presence of an impurity atom with a ~100% abundant $I=3/2$ nucleus, deduced indirectly from previous studies,[12] has been confirmed by the direct detection of its characteristic 4-line hyperfine structure in the ODMR spectrum of both the $A$ and $B$ configurations. The evidence for the involvement of copper in the defect, as previously suggested by these authors, is therefore confirmed.

(2) The symmetry for each defect configuration has been unambiguously established to be triclinic ($C_1$). This has been established both from the ODMR studies and the stress-splitting studies of the ZPL's for each configuration. This result serves to correct previous conclusions from ODMR studies that suggested higher ($C_{1h}$) symmetry for configuration $A$.[13]

(3) From the study of the optically induced $A\rightarrow B$ conversion, we have established that the energy dumped into the vibrational modes of defect $A$ when it luminesces does not supply a significant mechanism for the conversion. In addition, our results suggest that for below effective band-gap excitation, i.e., the phonon-assisted free exciton formation energy, direct optical excitation of the defect provides the dominant mechanism, as opposed to exciton capture, which has been argued to provide the dominant mechanism for excitation energies above the free exciton formation energy threshold.[9] Detailed study of the $B\rightarrow A$ recovery has established the thermal activation barrier to be $0.10\pm0.01$ eV. In either conversion study, the sum of the $A$ and $B$ concentrations, as monitored by their PL intensities, has been observed to be constant within experimental accuracy during the conversions. We have found no evidence therefore of a third intermediate and unseen configuration, as suggested in an earlier study.[8]

(4) Combining the $B\rightarrow A$ barrier with the energies for the optical transitions leads to a simple configurational diagram for the defect, as given in Fig. 3, locating the single donor level positions for the defect at $E_V+0.136$ eV and $E_V+0.291$ eV for $A$ and $B$, respectively, and with no other configuration involved. Evidence for an additional available negative charged state for the $A$ configuration has been presented by Chen *et al.*[9] but we have no direct evidence one way or the other on this question.

(5) Attempts to establish which is the stable configuration in the positive charge of the defect (equivalent to the excited EM state of the neutral state) were inconclusive due to an apparent difficulty in producing the defects in $p$-type material. The question therefore of *bistability* versus simple *metastability* has not been answered conclusively, and this final important feature required to fully complete the CC diagram remains uncertain.

(6) The general features of the ZPL stress-splitting results have been successfully modeled in terms of a Kaplyanskii piezospectroscopic tensor response for the deeply bound hole plus the deformation potential response for a Coulombically bound effective-mass-like electron. Two models have been presented, one with the effective mass $A_1$ state lowest, the other with the $E$ state lowest, each perturbed by the reduced symmetry of the defect core. The $E$ state supplies a significantly better match, but is less successful in accounting for the PLE spectra previously determined for the centers.

In conclusion, a great deal is now known concerning the defect. It involves an impurity with nuclear spin $I=3/2$, presumably copper, plus one or more sulfur atoms. It is a deep donor with two configurations between which it can cycle under optical excitation or thermal recovery at cryogenic temperatures and each has triclinic symmetry. Its luminescence results from a transition from its neutral excited effective-mass state to its ground deep neutral donor state for either configuration.

We still do not have, however, sufficient information to establish a detailed microscopic model for each of the configurations. Attempts at optical detection of ENDOR have not been successful, ruling out the valuable structural information that might be available from the additional magnetic and electric quadrupole information that it can often provide. However, a reasonable guess is that it involves a single substitutional sulfur atom paired off with an interstitial copper atom. That only a single sulfur atom is involved has been suggested by Brown *et al.*[2] who reported a linear dependence of the PL intensity with sulfur concentration. That it is substitutional is suggested by its bulk incorporation only after many hours at ~1200 °C. That the copper atom is interstitial is consistent with the rapid formation of the pair at ~700 °C, and also with the low migrational barrier required for one of the pair to account for the easy configurational changes of the complex at cryogenic temperatures. Consistent with this, we note the report[29] of easy reorientation at-cryogenic temperatures for the 1.0145-eV luminescence system, noted in Sec. I to display similar phonon structure to the $S$-related defect, and identified to be a Cu-Cu pair in silicon.

It is tempting therefore to consider as guides the models of other interstitial-substitutional pairs that have been identified to have similar metastability and for which detailed structures have been determined. These include interstitial carbon paired off with either substitutional carbon[30] or phosphorus.[31] In both cases, it is the interstitial carbon atom that hops from one nearby position to another, and the low symmetry arises from the fact that the interstitial atom nestles into bonded interstitialcy configurations with its neighbors, rather than occupy the tetrahedral interstitial site. We conclude that such a model represents the best present candidate for the $S$-related luminescence in silicon.

## ACKNOWLEDGMENTS

The research at Lehigh has been sponsored jointly by Office of Naval Research Grants No. N00014-90-J-1264 and N00014-94-1-0117, and National Science Foundation Grant No. DMR-92-04114. The research at King's College London has been supported by the Science and Engineering Research Council (SERC). We acknowledge financial support from SERC, making possible a 3 month visit by G.D.W. to King's College London for part of this work.

---

[*] Present address: Lucent Technologies, 9333 S. John Young Pkwy, Orlando, FL 32819.

[†] Present address: Philips Semiconductors, 9201 Pan American Fwy. NE, Albuquerque, NM 87113.

[‡] Present address: Fachbereich Physik der Phillips-Universität Marburg, 35032 Marburg, Germany.

[§] Present address: Center for Microelectronics Research, University of South Florida, 4202 Fowler Ave., Tampa, FL 33620.

[‖] Present address: Department of Physics, University of Jaffna, Jaffna, Sri Lanka.

[¶] Present address: Department of Materials Engineering, Brunel University, Uxbridge, Middlesex UB8 3PH, U.K.

[1] T.G. Brown and D.G. Hall, Appl. Phys. Lett. **49**, 245 (1986).

[2] P.L. Bradfield, T.G. Brown, and D.G. Hall, Phys. Rev. B **38**, 3533 (1988).

[3] A. Henry, E. Sörman, S. Andersson, W.M. Chen, B. Monemar, and E. Janźen, Phys. Rev. B **49**, 1662 (1994).

[4] E. Sörman, W.M. Chen, A. Henry, S. Andersson, E. Janźen, and B. Monemar, Phys. Rev. B **51**, 2132 (1995).

[5] D.J.S. Beckett, M.K. Nissen, and M.L.W. Thewalt, Phys. Rev. B **40**, 9618 (1989).

[6] P.J. Dean and D.C. Herbert, in *Excitons*, Topics in Current Physics Vol. 14, edited by K. Cho (Springer-Verlag, Berlin, 1979), p. 5555.

[7] M. Singh, E.C. Lightowlers, and G. Davies, Mater. Sci. Eng., B **4**, 303 (1989).

[8] A. Henry, W.M. Chen, E. Janzén, and B. Monemar, in *Proceedings of the 20th International Conference on the Physics of Semiconductors*, edited by E.M. Anastassakis and J.D. Joannopoulos (World Scientific, Singapore, 1990), p. 545.

[9] W.M. Chen, J.H. Svensson, E. Janzén, B. Monemar, A. Henry, A.M. Frens, M.T. Bennebroek, and J. Schmidt, Phys. Rev. Lett. **71**, 416 (1993).

[10] W.M. Chen, A. Henry, E. Janzén, B. Monemar, and M.L.W. Thewalt, in *Impurities, Defects and Diffusion in Semiconductors: Bulk and Layered Structures*, edited by D.J. Wolford, J. Bernholc, and E.E. Haller, MRS Symp. Proc. No. 163 (Materials Research Society, Pittsburgh, 1990), p. 303.

[11] W.M. Chen, M. Singh, A. Henry, E. Janzén, B. Monemar, A.M. Frens, M.T. Bennebroek, J. Schmidt, K.J. Reeson, and R.M. Gwilliam, Mater. Sci. Forum **83-87**, 251 (1992).

[12] A.M. Frens, M.T. Bennebroek, J. Schmidt, W.M. Chen, and B. Monemar, Phys. Rev. B **46**, 12 316 (1992).

[13] W.M. Chen, M. Singh, B. Monemar, A. Henry, E. Janzén, A.M. Frens, M.T. Bennebroek, and J. Schmidt, Phys. Rev. B **50**, 7365 (1994).

[14] L. Jeyanathan, G. Davies, E.C. Lightowlers, M. Singh, H.J. Sun, B. Ittermann, S.S. Ostapenko, W.A. Barry, P. Mason, and G.D. Watkins, Mater. Sci. Forum **143-147**, 1167 (1994).

[15] S.M. Sze, *Physics of Semiconductor Devices*, 2nd ed. (Wiley and Sons, New York, 1981), p. 69.

[16] W.M. Chen and B. Monemar, J. Appl. Phys. **68**, 2506 (1990).

[17] M.L.W. Thewalt and V.A. Karasyuk, Phys. Rev. Lett. **75**, 3962 (1995).

[18] W.M. Chen, B. Monemar, E. Janzén, A.M. Frens, M.T. Bennebroek, and J. Schmidt, Phys. Rev. Lett. **73**, 3258 (1994).

[19] W.M. Chen, B. Monemar, E. Janzén, A.M. Frens, M.T. Bennebroek, and J. Schmidt, Phys. Rev. Lett. **75**, 3963 (1995).

[20] G.D. Watkins, in *Deep Centers in Semiconductors*, edited by S.T. Pantelides (Gordon and Breach, New York, 1986), p. 175.

[21] G.D. Watkins, Mater. Sci. Forum **38-41**, 39 (1989).

[22] A.A. Kaplyanskii, Opt. Spektrosk. **16**, 602 (1994) [Opt. Spectrosc. **16**, 329 (1964)].

[23] M. Singh, G. Davies, E.C. Lightowlers, and G.D. Watkins, Mater. Sci. Forum **117-118**, 141 (1993).

[24] D.K. Wilson and G. Feher, Phys. Rev. **124**, 1068 (1961).

[25] V.J. Tekippe, H.R. Chandrasekar, P. Fisher, and A.K. Ramdas, Phys. Rev. B **6**, 2348 (1972).

[26] L. Jeyanathan, Ph.D. thesis, King's College London, 1994.

[27] C.P. Foy, J. Phys. C **15**, 2059 (1982).

[28] K. Thonke, A. Hangleiter, J. Wagner, and R. Sauer, J. Phys. C **18**, L795 (1985).

[29] J. Weber, H. Bauch, and R. Sauer, Phys. Rev. B **25**, 7688 (1982).

[30] L.W. Song, X.D. Zhan, B.W. Benson, and G.D. Watkins, Phys. Rev. B **42**, 5765 (1990).

[31] X.D. Zhan and G.D. Watkins, Phys. Rev. B **47**, 6363 (1993).